CONDENSED MATTER PHYSICS

# Generalized Anderson's theorem for superconductors derived from topological insulators

**Lionel Andersen[1]*, Aline Ramires[2,3,4]*†, Zhiwei Wang[1], Thomas Lorenz[1], Yoichi Ando[1]†**



**A well-known result in unconventional superconductivity is the fragility of nodal superconductors against nonmagnetic impurities. Despite this common wisdom, $Bi_2Se_3$-based topological superconductors have recently displayed unusual robustness against disorder. Here, we provide a theoretical framework that naturally explains what protects Cooper pairs from strong scattering in complex superconductors. Our analysis is based on the concept of superconducting fitness and generalizes the famous Anderson's theorem into superconductors having multiple internal degrees of freedom with simple assumptions such as the Born approximation. For concreteness, we report on the extreme example of the $Cu_x(PbSe)_5(BiSe_3)_6$ superconductor. Thermal conductivity measurements down to 50 mK not only give unambiguous evidence for the existence of nodes but also reveal that the energy scale corresponding to the scattering rate is orders of magnitude larger than the superconducting energy gap. This provides the most spectacular case of the generalized Anderson's theorem protecting a nodal superconductor.**

## INTRODUCTION

Unconventional superconductors distinguish themselves from conventional ones by breaking not only $U(1)$ gauge but also additional symmetries, usually reducing the point group associated with the normal-state electronic fluid. This extra symmetry reduction stems from the development of order parameters with nontrivial form factors, typically introducing point or line nodes in the excitation spectra. Nodal gap structures are especially known to give rise to power-law behavior in transport and thermodynamic quantities, which can be clearly detected in experiments, and are established as a key signature of unconventional superconductivity (*1*, *2*). However, nodal structures are also known to make superconductivity fragile in the presence of impurities, and many unconventional superconductors have actually been shown to be extremely sensitive to disorder (*3*, *4*).

Against all odds, the superconductivity in $Bi_2Se_3$-based materials was recently reported to present unusual robustness against disorder (*5*, *6*), despite showing nematic properties that point to unconventional topological superconductivity (*7*). Here, we report a notable observation that the $Cu_x(PbSe)_5(Bi_2Se_3)_6$ (CPSBS) superconductor (*8*), which also shows nematic properties (*9*), gives unambiguous evidence for the existence of gap nodes, while the scattering rate is more than an order of magnitude larger than the gap, a circumstance where nodal superconductivity is completely suppressed according to common wisdom. To understand this apparent puzzle, we generalize Anderson's theorem (*10*, *11*) to complex superconducting (SC) materials encoding extra internal degrees of freedom (DOF), such as orbitals, sublattices, or valleys. It turns out that as long as the pairing interaction is isotropic, superconductors having a momentum-dependent gap structure (which manifests itself in the band basis) are generically protected from nonmagnetic scattering that does not mix the internal DOF. Our analysis is performed in the Born approximation and is based on the concept of SC fitness (*12*, *13*), a useful tool for understanding the robustness of SC states involving multiple DOF.

## RESULTS

### Generalizing Anderson's theorem

We start generalizing Anderson's theorem to superconductors having extra internal DOF. To address the effects of impurities in such superconductors, it is useful to consider a Bogoliubov–de Gennes Hamiltonian

$$\widehat{H}_{\mathrm{BdG}}(\mathbf{k}) = \Psi_{\mathbf{k}}^{\dagger}\begin{pmatrix} \widehat{H}_0(\mathbf{k}) & \widehat{\Delta}(\mathbf{k}) \\ \widehat{\Delta}^{\dagger}(\mathbf{k}) & -\widehat{H}_0^{*}(-\mathbf{k}) \end{pmatrix}\Psi_{\mathbf{k}} \tag{1}$$

written in terms of a multi-DOF Nambu spinor $\Psi_{\mathbf{k}}^{\dagger} = (\Phi_{\mathbf{k}}^{\dagger}, \Phi_{-\mathbf{k}}^{T})$, encoding several DOF within $\Phi_{\mathbf{k}}^{\dagger} = (c_{1\mathbf{k}\uparrow}^{\dagger}, c_{1\mathbf{k}\downarrow}^{\dagger}, \ldots, c_{n\mathbf{k}\uparrow}^{\dagger}, c_{n\mathbf{k}\downarrow}^{\dagger})$. Here, $c_{m\mathbf{k}\sigma}^{\dagger}$ ($c_{m\mathbf{k}\sigma}$) creates (annihilates) an electron in the internal DOF $m$ with momentum $\mathbf{k}$, and spin $\sigma = \{\uparrow, \downarrow\}$. $\widehat{H}_0(\mathbf{k})$ is the normal-state Hamiltonian in this multi-DOF basis, which can be parametrized as

$$\widehat{H}_0(\mathbf{k}) = \sum_{a,b} h_{ab}(\mathbf{k})\,[\hat{\tau}_a \otimes \hat{\sigma}_b] \tag{2}$$

where $h_{ab}(\mathbf{k})$ are momentum-dependent real functions with subscripts $a$ and $b$ corresponding to the extra internal DOF and the spin DOF, respectively. If we focus on the case of two orbitals as the extra internal DOF (as in the $Bi_2Se_3$-based superconductors), then $\hat{\tau}_i$ and $\hat{\sigma}_i$ ($i = \{1,2,3\}$) are the Pauli matrices to encode the orbital and spin DOFs, respectively, and $\hat{\tau}_0$ and $\hat{\sigma}_0$ are identity matrices. In the most general case, there are 16 parameters $h_{ab}(\mathbf{k})$. However, in the presence of time-reversal and inversion symmetries, the number of allowed $h_{ab}(\mathbf{k})$ terms is reduced to only five plus $h_{00}(\mathbf{k})$, with the associated matrices $\hat{\tau}_a \otimes \hat{\sigma}_b$ forming a set of totally anticommuting matrices.

In Eq. 1, $\widehat{\Delta}(\mathbf{k})$ is the gap matrix, which can be parametrized in a similar form

$$\widehat{\Delta}(\mathbf{k}) = \sum_{a,b} d_{ab}(\mathbf{k})\,[\hat{\tau}_a \otimes \hat{\sigma}_b(i\hat{\sigma}_2)] \tag{3}$$

[1]Physics Institute II, University of Cologne, 50937 Köln, Germany. [2]Max Planck Institute for the Physics of Complex Systems, Dresden, 01187, Germany. [3]ICTP-SAIFR, International Centre for Theoretical Physics–South American Institute for Fundamental Research, São Paulo, SP 01140-070, Brazil. [4]Instituto de Física Teórica–Universidade Estadual Paulista, São Paulo, SP 01140-070, Brazil.
*These authors contributed equally.
†Corresponding author. Email: aline.ramires@ictp-saifr.org (A.R.); ando@ph2.uni-koeln.de (Y.A.)

Here, $d_{ab}(\mathbf{k})$ denote form factors, which, in general, can have a $\mathbf{k}$ dependence determined by the pairing mechanism. However, when superconductivity is driven by phonons or by local interactions, the pairing force is isotropic and $d_{ab}$ becomes independent of $\mathbf{k}$. Previous works have shown that conventional electron-phonon coupling in the presence of Coulomb repulsion is a possible mechanism to drive odd-parity superconductivity in $Bi_2Se_3$-based superconductors (*14*, *15*). In the following, we focus on $\mathbf{k}$-independent $d_{ab}$ and show that this assumption allows for a consistent description of the phenomenology of this family of materials.

The effects of impurities in multi-DOF superconductors can be understood by calculations similar in spirit as the standard calculations for simple metals within the Born approximation (*11*) (see details in section S1), from which we can infer the behavior of the critical temperature, $T_c$, as a function of the effective scattering rate $\hbar\Gamma_{\mathrm{Eff}}$ associated with depairing mechanisms. The calculations yield a familiar result, which is now generalized to encode the complexity of the normal and SC states in the multi-DOF basis

$$\log\left(\frac{T_c}{T_c^0}\right) = \Psi\left(\frac{1}{2}\right) - \Psi\left(\frac{1}{2}+\frac{\hbar\Gamma_{\mathrm{Eff}}}{2\pi k_B T_c}\right) \quad (4)$$

where $T_c^0$ is the critical temperature of the clean system, $\Psi(x)$ is the digamma function, and $\hbar\Gamma_{\mathrm{Eff}}$ encodes all pair-breaking mechanisms through

$$\hbar\Gamma_{\mathrm{Eff}} = \frac{1}{4}\left\langle \overline{Tr\left[\tilde{F}_C^{\dagger}(\Omega_{\mathbf{k}})\,\tilde{F}_C(\Omega_{\mathbf{k}})\right]}\right\rangle_{\mathbf{k}} \quad (5)$$

which is determined solely by the SC fitness function (*12*, *13*)

$$\hat{F}_C(\mathbf{k}-\mathbf{k}') = \hat{V}(\mathbf{k}-\mathbf{k}')\,\hat{\Delta} - \hat{\Delta}\,\hat{V}^*(\mathbf{k}-\mathbf{k}') \quad (6)$$

This expression is valid for $\mathbf{k}$-independent $\hat{\Delta}$ matrices of arbitrary dimension. Here, $\hat{V}(\mathbf{k}-\mathbf{k}')$ is the matrix impurity scattering potential encoding all DOFs, $\tilde{F}_C(\Omega_{\mathbf{k}}) = \hat{F}_C(\Omega_{\mathbf{k}})/\Delta_0$, $\Delta_0$ is the magnitude of the gap, $\Omega_{\mathbf{k}}$ is the solid angle at the Fermi surface, the horizontal bar indicates impurity averaging, and the brackets indicate the average over the Fermi surface. This form of effective scattering rate accounts for the potentially nontrivial dependences of the pair wave functions and different scattering processes among the multiple DOFs through the SC fitness function $\hat{F}_C(\mathbf{k})$. It is prudent to mention that the SC fitness concept was originally introduced as a measure of the incompatibility of the normal-state electronic structure with the gap matrix (*12*, *13*). The effects of disorder on the SC state can also be inferred directly from the SC fitness function, if one introduces an impurity scattering potential to the normal-state Hamiltonian.

On the basis of Eqs. 4 to 6, we can now formulate the generalized Anderson's theorem as follows: For a momentum-independent SC order parameter in the orbital basis encoded by the matrix $\hat{\Delta}$, the SC state is robust against impurities if the associated scattering potential $\hat{V}(\mathbf{k}-\mathbf{k}')$ in the orbital basis satisfies

$$\hat{F}_C(\mathbf{k}-\mathbf{k}') = 0 \quad (7)$$

This condition recovers Anderson's original result in the one band limit (in which case a nonmagnetic scattering potential is proportional to the identity) but now allows us to address more complex materials with extra internal DOF. As will be shown in the next section, for a scenario in which inter-DOF scattering is not allowed, Anderson's theorem can still hold even if the gap has nodes when projected to the Fermi surface.

## Robust superconductivity in the $Bi_2Se_3$-based materials

We can now use the fitness function to discuss the robustness of the SC state observed in the $Bi_2Se_3$-based materials. The normal state can be described by focusing on the quintuple-layer (QL) units, as schematically depicted in Fig. 1. The QL has $D_{3d}$ point group symmetry, and the low-energy electronic structure can be described by an effective two-orbital model (*16*). The orbitals stem from Bi and Se atoms and have $p_z$ character. By a combination of hybridization, crystal field effects, and spin-orbit coupling, one can identify two effective orbitals with opposite parity, labeled $P_{1z+}$ and $P_{2z-}$, with the ± sign indicating the parity (*17*). A schematic representation of the orbitals is given in Fig. 1B. With the definition $\Phi_{\mathbf{k}}^{\dagger} = (c_{1\uparrow}^{\dagger}, c_{1\downarrow}^{\dagger}, c_{2\uparrow}^{\dagger}, c_{2\downarrow}^{\dagger})_{\mathbf{k}}$, the normal-state Hamiltonian can be parametrized as Eq. 2. In the presence of time-reversal and inversion symmetries, only the terms with $(a, b) = \{(0,0), (2,0), (3,0), (1,1), (1,2), (1,3)\}$ are allowed in the

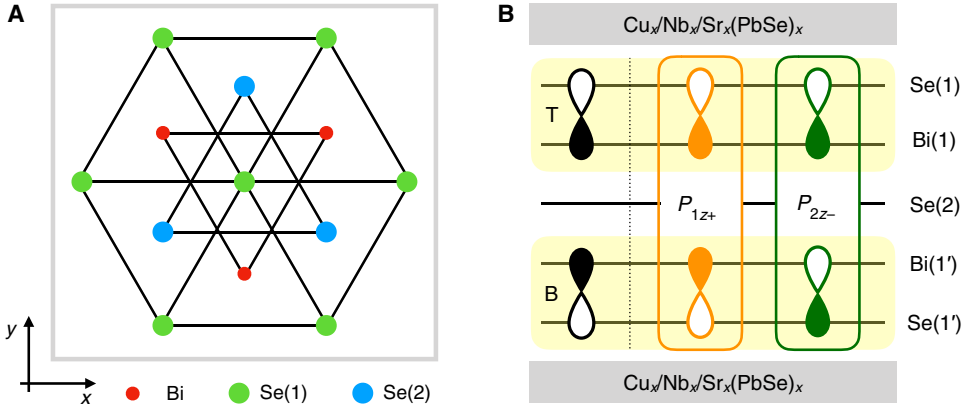


**Fig. 1. Material under consideration.** (**A**) Schematic representation of the crystal structure for materials in the family of $Bi_2Se_3$ (view along the *c* axis); the gray rectangle depicts the reduced (monoclinic) symmetry in CPSBS (see discussion in section S4). (**B**) Side view of the QL unit, highlighting the specific choice of orbitals: Shown on the left are the top (T) and bottom (B) layer orbitals used in (*18*); shown on the right are the even ($P_{1z+}$) and odd ($P_{2z-}$) parity orbitals used in this work, identified as symmetric and antisymmetric superpositions of the orbitals in the top/bottom layers.

Hamiltonian. The properties of the respective matrices under the point group operations allow us to associate each of these terms to a given irreducible representation of $D_{3d}$, therefore constraining the momentum dependence of the form factors $h_{ab}(\mathbf{k})$. More details on the parametrization of the Hamiltonian are given in section S2.

The gap matrix can be parametrized as in Eq. 3 in the orbital basis. As already noted, we focus on $\mathbf{k}$-independent $\hat{\Delta}$ matrices in this basis because the pairing force is considered to be isotropic in $Bi_2Se_3$-based superconductors (*14*, *15*, *18*). Within the $D_{3d}$ point group symmetry, the allowed order parameters are summarized in table S2. In Fig. 2A, we provide a schematic representation of pairing in the orbital basis, in which one can distinguish intraorbital pairing in the even $A_{1g}$ channel from interorbital pairing in the odd channels (*19*). Given the experimental evidence for nodes along the $y$ direction in CPSBS (*9*), here we focus on the following $E_u$ order parameter:

$$\hat{\Delta} = \Delta_0[i\hat{\tau}_2 \otimes \hat{\sigma}_1(i\hat{\sigma}_2)] = \Delta_0 \begin{pmatrix} 0 & 0 & -1 & 0 \\ 0 & 0 & 0 & 1 \\ 1 & 0 & 0 & 0 \\ 0 & -1 & 0 & 0 \end{pmatrix} \quad (8)$$

which is spin triplet and orbital singlet. Under the action of the parity operator $\hat{P} = \hat{\tau}_3 \otimes \hat{\sigma}_0$, one can infer that this is an odd-parity state, even though the gap matrix is momentum independent. The oddness of this order parameter stems from the different parity of the two underlying orbitals. This $\mathbf{k}$-independent order parameter in the orbital basis acquires nodes along the $y$ axis once projected to the Fermi surface in the band basis (as shown schematically in Fig. 2B; see section S3 for explicit calculations).

Given the order parameter from Eq. 8, we can now use the SC fitness function to understand the robustness of the SC state in CPSBS. We write the explicit form of the matrix impurity scattering potential $\hat{V}(\mathbf{k}-\mathbf{k}')$ as

$$\hat{V}(\mathbf{k}-\mathbf{k}') = [V_0(\mathbf{k}-\mathbf{k}')\hat{\tau}_0 \otimes \hat{\sigma}_0 + V_s(\mathbf{k}-\mathbf{k}')\mathbf{S}\cdot(\hat{\tau}_0 \otimes \hat{\boldsymbol{\sigma}})] \quad (9)$$

where $V_a(\mathbf{k}-\mathbf{k}')$ is the Fourier transform of the scattering potential introduced by a localized impurity in real space. Here, $a = \{0, s\}$ indicates nonmagnetic and magnetic impurity scattering, respectively; $\mathbf{S}$ signifies the spin of the magnetic impurities, and $\hat{\boldsymbol{\sigma}}$ the spin of the scattered electrons. The key aspect of the scattering potential for this material is the absence of orbital mixing, namely, no terms with $\hat{\tau}_1$ or $\hat{\tau}_2$ contributions. This is guaranteed by the opposite parity of the effective orbitals within the assumption of an inversion symmetric impurity potential. Another key aspect is the fact that the two orbitals are symmetric and antisymmetric combinations of the same two orbitals in the top/bottom layers; therefore, there is also no $\hat{\tau}_3$ term in the scattering potential (since it would imply that the scattering amplitude for the two effective orbitals is different). Under these circumstances, the scattering potential can only have the simple form given above.

Note that the scattering associated with nonmagnetic impurities is rather trivial in its matrix form, $\sim\hat{\tau}_0 \otimes \hat{\sigma}_0$, which always commute with the gap matrices $\hat{\Delta}$. As a consequence, the generalized Anderson's theorem, as formulated in Eq. 7, is satisfied, and the effective scattering rate for nonmagnetic impurities in CPSBS with the SC order parameter in the $E_u$ channel is zero, even though the gap changes sign across the nodes, which are present in this $E_u$

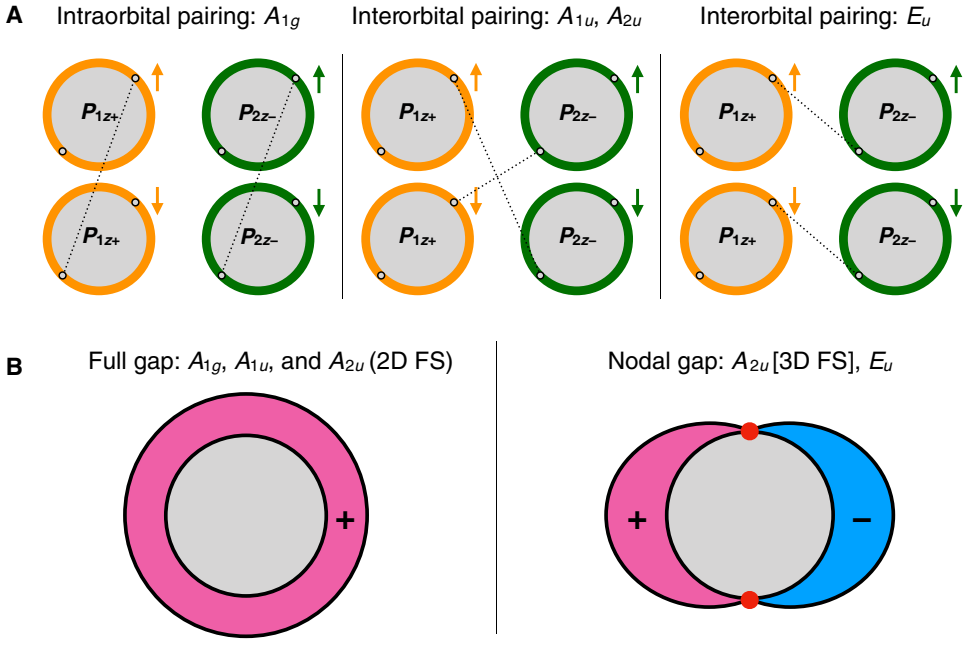


**Fig. 2. Possibilities of pairing.** (**A**) Schematic representation of the gap structure in the orbital basis. The yellow and green colors correspond to $P_{1z+}$ and $P_{2z-}$ orbitals, respectively, as shown in Fig. 1 (**B**). The dotted lines represent pairing between electrons with opposite momenta. Left: Intraorbital singlet pairing for $A_{1g}$. Middle: Interorbital triplet/singlet pairing for $A_{1u}/A_{2u}$. Right: Interorbital triplet pairing for $E_u$. (B) Schematic representation of the gap function in the band basis. Left: Fully gapped, for order parameters in $A_{1g}$ and $A_{1u}$, as well as in $A_{2u}$ for a two-dimensional (2D) Fermi surface (FS). Right: Nodal gap structure for order parameters in $A_{2u}$ (for a 3D FS) and $E_u$. The red dot indicates the position of the nodes, which can be read off from table S3. For a 3D FS, these are point nodes on an ellipsoidal FS, while for a 2D FS, these are line nodes extending along the $z$ direction on a cylindrical FS.

channel. Note that in this theoretical framework, the gap nodes are induced by the normal-state band structure once one translates the problem from the orbital basis to the band basis, as schematically shown in Fig. 2B and discussed in detail in section S3. The conclusion of zero scattering rate is valid for any momentum-independent SC order parameter possible for the $Bi_2Se_3$-based materials because the identity matrix $\hat{\tau}_0 \otimes \hat{\sigma}_0$ commutes with any $\hat{\Delta}$ of the form $\hat{\tau}_a \otimes \hat{\sigma}_b$.

Previous theoretical works have discussed unexpected effects of impurities in multiband and multiorbital superconductors, mostly focusing on Fe-based superconductors with $s_{++}$ or $s_{+-}$ SC states, which ultimately belong to the trivial irreducible representation of the respective point group (*20*, *21*). Here, we proposed a novel scenario, in which order parameters in a nontrivial irreducible representation displaying symmetry-protected nodes are shown to be robust against disorder. In the context of superconductors derived from $Bi_2Se_3$, Michaeli and Fu discussed how spin-orbit locking could parametrically protect unconventional SC states, but their results are valid only for states with pairs of electrons of the same chirality, restricting the analysis to order parameters in the $A_{1g}$ and $A_{1u}$ representations (*22*). More recently, Nagai proposed that the interorbital spin-triplet state with $E_u$ symmetry can be mapped to an intraorbital spin-singlet s-wave pairing if the roles of spin and orbital are exchanged in the Hamiltonian, and he argued that this mapping could provide a mechanism for Anderson's theorem to remain valid in the presence of strong spin-orbit coupling (*23*). Both works rely on assumptions that are not valid for all SC symmetry channels and depend on strong spin-orbit coupling. These restrictions are not required for the above generalization of Anderson's theorem for multi-DOF superconductors, which shows that the robustness of the SC state against impurities is guaranteed by the isotropic nature of the pairing interaction written in the local orbital basis (leading to a momentum-independent order parameter in this microscopic basis), under the requirement that impurity scattering is not allowed between orbitals with opposite parity. These considerations are concisely captured by the SC fitness function $\hat{F}_C(\boldsymbol{k})$. We emphasize that this framework has a particular importance in the context of topological superconductors because the topological nature is often endowed by the extra DOF (*7*).

## The case of CPSBS

CPSBS is a superconductor obtained by intercalating Cu into its parent compound $(PbSe)_5(Bi_2Se_3)_6$, which is a member of the $(PbSe)_5(Bi_2Se_3)_{3m}$ homologous series realizing a natural heterostructure formed by a stack of the trivial insulator PbSe and the topological insulator $Bi_2Se_3$ (*8*). It was recently elucidated (*9*) that CPSBS belongs to the class of unconventional superconductors derived from $Bi_2Se_3$, including $Cu_xBi_2Se_3$ (*7*), $Sr_xBi_2Se_3$ (*24*, *25*), and $Nb_xBi_2Se_3$ (*26*, *27*), that have a topological odd-parity SC state, which spontaneously breaks rotation symmetry (*28*). In contrast to the fully opened gap in $Cu_xBi_2Se_3$ (*29*), the gap in CPSBS appears to have symmetry-protected nodes (*9*).

Figure 3A shows the temperature dependence of the electronic specific heat $c_{el}$, which is obtained from the total specific heat $c_p$ by subtracting the phononic contribution $c_{ph}$ (*9*), for the two samples studied in this work. The line-nodal gap theory (*30*) describes the $c_{el}(T)$ data well, and the fits using this theory allow us to estimate the SC volume fraction, which is 85 and 100% for samples I and II, respectively. The thermal conductivity $\kappa$ was measured on the same samples down to 50 mK (Figs. 3B and 4) with the configuration depicted in Fig. 3C. Note that our previous study of $c_p$ in CPSBS in rotating magnetic field has revealed that line nodes are located in the *a* direction (*9*). The $c_p(T)$ data in the normal state obey $c_p = \gamma_{el}T + \beta_{ph}T^3$ (*9*), and we extract the phononic specific-heat coefficient $\beta_{ph} = 5.1$ (5.2) mJ/molK$^4$ and the electronic specific-heat coefficient $\gamma_{el} = 5.8$ (6.9) mJ/molK$^2$ for sample I (II). The $\kappa/T$ data present no anomaly at $T_c$ (Fig. 3B), suggesting that electron-electron scattering is not dominant.

In the $\kappa(T)$ data, one can separate the phononic and the electronic contributions to the heat transport when the $\kappa/T$ versus $T^2$ plot shows a linear behavior at low enough temperature. In our samples, this happens for $T \lesssim 100$ mK (Fig. 4, A and B), where phonons enter the boundary scattering regime and the phononic thermal conductivity $\kappa_{ph}$ changes as $b_{ph}T^3$ (see the Supplementary Materials). A finite intercept of the linear behavior in this plot means that there is a residual electronic thermal conductivity $\kappa_0$ that originated from residual quasiparticles, whose contribution increases linearly with $T$, i.e., $\kappa_0 = a_eT$. In nodal superconductors, it has been established (*1*) that impurity scattering gives rise to a finite density of residual quasiparticles even at zero temperature, which is responsible for the finite $a_e$. Upon application of a magnetic field $H$, vortices create additional quasiparticles that affect $\kappa$. In both samples, the magnetic-field dependence of $a_e$ is sublinear (see Fig. 4, C and D), and this is most likely due to the Doppler shift of the superfluid around vortices, which leads to a $\sim\sqrt{H}$ increase in $c_{el}$ in a nodal superconductor (*31*). Note that the exact $H$ dependence of $a_e$ would not be simple because vortices enhance both the quasiparticle density and their scattering rate (*32*). In 2.5 T, the superconductivity is fully suppressed, and the $\kappa/T$ data are those of the normal state.

At this point, it is important to notice that these $\kappa/T$ data unambiguously show the presence of residual mobile quasiparticles down to 50 mK, which gives convincing evidence for the existence of gap nodes. In particular, sample II is essentially 100% SC as indicated by the $c_p$ data, and yet, this sample in 0 T shows significant electronic heat conduction in the zero-temperature limit, which accounts for ~24% of the normal-state heat conduction (see Fig. 4D). This is impossible for a fully gapped superconductor. The case for sample I is similar: Although the SC volume fraction of this sample is ~85% and hence one would expect some residual heat conduction at the level of 15% of the normal-state value (shown by the hatch at the bottom of Fig. 4C) due to the non-SC portion of the sample, the actual residual heat conduction in 0 T accounts for ~45% of the normal-state

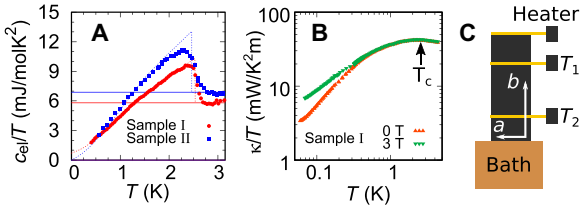


**Fig. 3. Specific heat and thermal conductivity across $T_c$.** (**A**) Temperature dependencies of the electronic specific heat $c_{el}$ of samples I and II (symbols), together with the theoretical curve for a line-nodal SC gap in the clean limit (*30*) assuming the SC volume fraction of 85 and 100%, respectively; horizontal lines correspond to $\gamma_{el}$. Note that despite the strong scatterings in these samples, the clean-limit theory describes the $c_{el}(T)$ data well, which is related to the robustness of the SC state against impurities. (**B**) Double-logarithmic plot of $\kappa/T$ versus $T$ for sample I measured in 0 and 3 T. (**C**) Schematics of the steady-state thermal-conductivity measurement setup.

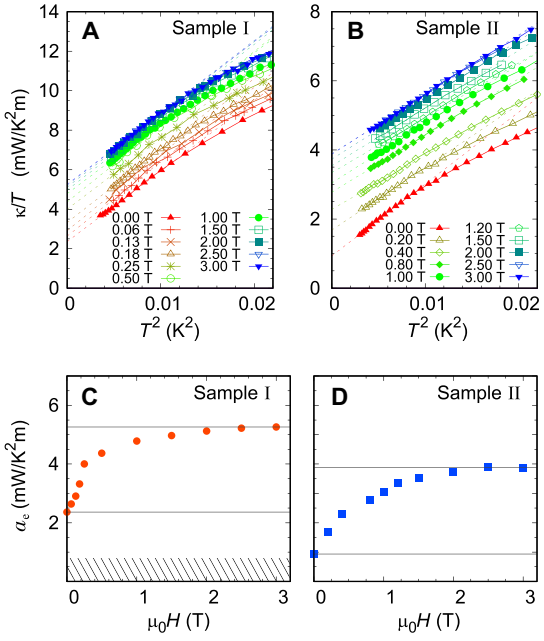


**Fig. 4. Ultralow-temperature thermal conductivity.** (**A** and **B**) Plots of $\kappa/T$ versus $T^2$ for samples I and II measured in perpendicular magnetic fields up to 3 T. Dashed lines are the linear fits to the lowest-temperature part of the data; the intercept of these lines on the $\kappa/T$ axis gives $\kappa_0/T$. (**C** and **D**) Magnetic-field dependencies of the electronic heat-transport coefficient $a_e$ in samples I and II; solid lines mark the range of its change from 0 T to the normal state. The hatch at the bottom of (C) represents the expected background contributed by the non-SC portion of sample I.

value, which strongly points to the contribution of residual nodal quasiparticles.

## DISCUSSION

To put the observed magnitude of κ into context, the Wiedemann-Franz law $\kappa_0/T = L_0/\rho_{res}$ is useful ($L_0 = \frac{\pi^2}{3}k_B^2/e^2 = 2.44 \times 10^{-8}$ ΩW/K$^2$ is the Sommerfeld value of the Lorenz number, and $\rho_{res}$ is the residual resistivity). Using this formula and the observed $\kappa_0/T$ values in the normal state, we obtain $\rho_{res}$ of 4.6 and 6.3 μΩm for samples I and II, respectively, which compares well to the direct measurements of $\rho_{res}$ (*8*). We now make an order-of-magnitude estimate of the scattering time τ from $\rho_{res}$ using the simple Drude model $\rho_{res} = m^*/(ne^2\tau)$ and the relation between the effective mass $m^*$ and $\gamma_{el}$ for a two-dimensional free electron gas. With $\gamma_{el} = 6.9$ mJ/molK$^2$ of sample II, one obtains $m^* = (3\hbar^2\gamma_{el}c_0)/(\pi V_{mol}k_B^2) = 4.7m_e$, where $V_{mol} = 115.8$ cm$^3$/mol is the $Bi_2Se_3$ molar volume used for the normalization of $c_p$, and $c_0 = 1.27$ nm is the height of the corresponding unit cell. With the typical carrier density $1.2 \times 10^{21}$ cm$^{-3}$ in CPSBS (*8*), one obtains $\tau = 2.2 \times 10^{-14}$ s for sample II. Since $m^* = 4.7m_e$ obtained from $\gamma_{el}$ is likely an overestimate of the transport effective mass, it only gives an upper bound for τ. Hence, we obtain a lower bound of the scattering rate $\hbar\Gamma = \hbar/\tau = 30$ meV, which is already more than an order of magnitude larger than the SC gap $\Delta_0 \simeq 0.5$ meV. We note that the mobility in CPSBS is only ~10 cm$^2$/Vs, which precludes the determination of $m^*$ from quantum oscillations, although $m^* \simeq 0.2m_e$ has been estimated from quantum oscillations in $Cu_xBi_2Se_3$ (*33*) and $Nb_xBi_2Se_3$ (*34*). Note that, if the actual effective mass is lighter than $4.7m_e$ in CPSBS, then $\hbar\Gamma$ becomes larger, and the conclusion about the robustness becomes even stronger. The estimates of $\hbar\Gamma$ for other $Bi_2Se_3$-based superconductors from the same Drude analyses unanimously give values larger than $\Delta_0$ [see section S5 and (*24*, *35*–*37*)], indicating the universal nature of the robustness in this family of unconventional superconductors.

It is crucial to notice that the universal thermal conductivity (*38*–*40*), which is expected only in clean superconductors satisfying $\hbar\Gamma \ll \Delta_0$, is not observed here. A simple estimate of the expected magnitude of the universal thermal conductivity $\kappa_0^{univ}$ given by $\kappa_0^{univ}/T \approx (\gamma_{el}v_F^2\hbar)/(2V_{mol}\Delta_0)$ (*39*) makes this situation clear: By using the Fermi velocity $v_F = 4.8 \times 10^5$ m/s obtained from the angle-resolved photoemission experiments on CPSBS (*41*), one finds $\kappa_0^{univ}/T \approx 8$ W/K$^2$ m, which is three orders of magnitude larger than the actual $\kappa_0/T$ in CPSBS in 0 T, indicating that the $\kappa_0/T$ value is significantly reduced from its clean-limit value due to strong impurity scattering. This gives convincing evidence that the strong scattering corresponding to $\hbar\Gamma \gg \Delta_0$ is at work not only in the normal state but also in the SC state. Note that in high-$T_c$ cuprates, the strong scattering leading to the "bad metal" behavior in the normal state is suppressed in the SC state, leading to the universal thermal conductivity to be observed in the mK region; clearly, this is not the case here.

Hence, one can safely conclude that in CPSBS, the energy scale of the scattering rate is much larger than the SC gap, which would normally preclude the realization of unconventional superconductivity with a nodal gap. This provides a spectacular proof of the generalized Anderson's theorem in a multi-DOF superconductor. It is useful to note that the unusual robustness in $T_c$ against disorder was already noted for $Cu_xBi_2Se_3$ (*5*) and $Nb_xBi_2Se_3$ (*6*), and the penetration-depth measurements of $Nb_xBi_2Se_3$ also found evidence for nodes (*42*), but the origin of the robustness remained a mystery. This mystery has actually been a reason for hindering part of the community from accepting $Bi_2Se_3$-based materials as well-established unconventional superconductors. The present work finally solved this mystery, and it further provides a new paradigm for understanding the robustness of unconventional superconductivity. The new framework presented here will form the foundation for understanding the superconductivity in novel quantum materials where extra internal DOF such as orbitals, sublattices, or valleys govern the electronic properties.

## MATERIALS AND METHODS

High-quality CPSBS single crystals were grown by a modified Bridgman method as described before (*9*). Two samples from the same growth batch were measured. The dimensions of samples I and II were 2.8 mm by 2.5 mm by 0.35 mm and 5.6 mm by 2.0 mm by 0.20 mm, respectively. The exact $x$ values of samples I and II were 1.47 and 1.29, respectively. The specific heat $c_p$ was measured with a relaxation method in a Quantum Design PPMS down to 300 mK. Following previous works on CPSBS (*8*, *9*), the SC volume fraction was estimated from the $c_p$ data by subtracting the phononic contribution $c_{ph}$ and fitting the electronic contribution $c_{el}$ with a line-nodal gap theory (*30*), yielding 85 and 100% for samples I and II, respectively. The shielding fraction at 1.8 K measured with a SQUID magnetometer in 0.2 mT applied parallel to the *ab* plane was 75 and 88% in samples I and II, respectively. The thermal conductivity κ was measured on the same samples in a dilution refrigerator (Oxford Instruments Kelvinox 400) with the standard steady-state method

depicted in Fig. 3C in the main text using $RuO_2$ thermometers. The temperature gradient $\nabla T$ was applied parallel to the $b$ axis, and the magnetic field was applied along the $c^*$ axis; note that CPSBS belongs to the $C2/m$ space group, where $\vec{a} \perp \vec{b}$ and $\vec{c}^* \parallel \vec{a} \times \vec{b}$.

## SUPPLEMENTARY MATERIALS

Supplementary material for this article is available at http://advances.sciencemag.org/cgi/content/full/6/9/eaay6502/DC1

Section S1. The concept of SC fitness and the effective scattering rate
Section S2. The normal-state Hamiltonian for materials in the family of $Bi_2Se_3$
Section S3. The order parameters for materials in the family of $Bi_2Se_3$
Section S4. Analysis for $C_{2h}$ symmetry
Section S5. Drude analysis of the scattering rates in $Bi_2Se_3$-based superconductors
Section S6. Phononic contribution to the thermal conductivity
Table S1. Parametrization of the normal-state Hamiltonian.
Table S2. Superconducting order parameters for the materials in the family of $Bi_2Se_3$.
Table S3. Analysis of the gap structure for the materials in the family of $Bi_2Se_3$.
Table S4. Estimates of the scattering rates in $Bi_2Se_3$-based superconductors from the simple Drude analysis as was done for CPSBS in the main text.
Fig. S1. Behavior of phonons.

## REFERENCES AND NOTES


1. N. E. Hussey, Low-energy quasiparticles in high-$T_c$ cuprates. *Adv. Phys.* **51**, 1685–1771 (2002).
2. H. Shakeripour, C. Petrovic, L. Taillefer, Heat transport as a probe of superconducting gap structure. *New J. Phys.* **11**, 055065 (2009).
3. A. P. Mackenzie, R. K. W. Haselwimmer, A. W. Tyler, G. G. Lonzarich, Y. Mori, S. Nishizaki, Y. Maeno, Extremely strong dependence of superconductivity on disorder in $Sr_2RuO_4$. *Phys. Rev. Lett.* **80**, 161–164 (1998).
4. Y. Dalichaouch, M. C. de Andrade, D. A. Gajewski, R. Chau, P. Visani, M. B. Maple, Impurity scattering and triplet superconductivity in $UPt_3$. *Phys. Rev. Lett.* **75**, 3938–3941 (1995).
5. M. Kriener, K. Segawa, S. Sasaki, Y. Ando, Anomalous suppression of the superfluid density in the $Cu_xBi_2Se_3$ superconductor upon progressive Cu intercalation. *Phys. Rev. B* **86**, 180505(R) (2012).
6. M. P. Smylie, K. Willa, H. Claus, A. Snezhko, I. Martin, W. K. Kwok, Y. Qiu, Y. S. Hor, E. Bokari, P. Niraula, A. Kayani, V. Mishra, U. Welp, Robust odd-parity superconductivity in the doped topological insulator $Nb_xBi_2Se_3$. *Phys. Rev. B* **96**, 115145 (2017).
7. M. Sato, Y. Ando, Topological superconductors: A review. *Rep. Prog. Phys.* **80**, 076501 (2017).
8. S. Sasaki, K. Segawa, Y. Ando, Superconductor derived from a topological insulator heterostructure. *Phys. Rev. B* **90**, 220504 (2014).
9. L. Andersen, Z. Wang, T. Lorenz, Y. Ando, Nematic superconductivity in $Cu_{1.5}(PbSe)_5(Bi_2Se_3)_6$. *Phys. Rev. B* **98**, 220512(R) (2018).
10. P. W. Anderson, Theory of dirty superconductors. *J. Phys. Chem. Solid* **11**, 26–30 (1959).
11. K. Maki, Gapless superconductivity, in *Superconductivity: Part II*, R. D. Parks, Ed. (Marcel Dekker Inc., New York, 1969).
12. A. Ramires, M. Sigrist, Identifying detrimental effects for multiorbital superconductivity: Application to $Sr_2RuO_4$. *Phys. Rev. B* **94**, 104501 (2016).
13. A. Ramires, D. F. Agterberg, M. Sigrist, Tailoring $T_c$ by symmetry principles: The concept of superconducting fitness. *Phys. Rev. B* **98**, 024501 (2018).
14. F. Wu, I. Martin, Nematic and chiral superconductivity induced by odd-parity fluctuations. *Phys. Rev. B* **96**, 144504 (2017).
15. P. M. R. Brydon, S. Das Sarma, H.-Y. Hui, J. D. Sau, Odd-parity superconductivity from phonon-mediated pairing: Application to $Cu_xBi_2Se_3$. *Phys. Rev. B* **90**, 184512 (2014).
16. For the specific case of CPSBS, the $(PbSe)_5$ layers actually have square symmetry, such that the entire structure has the reduced point group symmetry $C_{2h}$. This is represented by the gray square in Fig. 1A. More details in section S4.
17. C.-X. Liu, X.-L. Qi, H. Zhang, X. Dai, Z. Fang, S.-C. Zhang, Model hamiltonian for topological insulators. *Phys. Rev. B* **82**, 045122 (2010).
18. L. Fu, E. Berg, Odd-parity topological superconductors: Theory and application to $Cu_xBi_2Se_3$. *Phys. Rev. Lett.* **105**, 097001 (2010).
19. Note that the explicit form of the order parameters differ from the ones in Fu and Berg (*18*). The character of the orbitals is different from our formalism, which is evident from the form of the parity operator. Here, we choose to start with a basis in which the parity operator is diagonal, which led to the insights described here. The two descriptions are in fact consistent and are related by a unitary transformation (*17*).
20. M. S. Scheurer, M. Hoyer, J. Schmalian, Pair breaking in multiorbital superconductors: An application to oxide interfaces. *Phys. Rev. B* **92**, 014518 (2015).
21. M. M. Korshunov, Y. N. Togushova, O. V. Dolgov, Impurities in multiband superconductors. *Physics-Uspekhi* **59**, 1211–1240 (2016).
22. K. Michaeli, L. Fu, Spin-orbit locking as a protection mechanism of the odd-parity superconducting state against disorder. *Phys. Rev. Lett.* **109**, 187003 (2012).
23. Y. Nagai, Robust superconductivity with nodes in the superconducting topological insulator $Cu_xBi_2Se_3$: Zeeman orbital field and nonmagnetic impurities. *Phys. Rev. B* **91**, 060502 (2015).
24. Z. Liu, X. Yao, J. Shao, M. Zuo, L. Pi, S. Tan, C. Zhang, Y. Zhang, Superconductivity with topological surface state in $Sr_xBi_2Se_3$. *J. Am. Chem. Soc.* **137**, 10512–10515 (2015).
25. Y. Pan, A. M. Ikitin, G. K. Araizi, Y. K. Huang, Y. Matsushita, T. Naka, A. de Visser, Rotational symmetry breaking in the topological superconductor $Sr_xBi_2Se_3$ probed by upper-critical field experiments. *Sci. Rep.* **6**, 28632 (2016).
26. J. Shen, W.-Y. He, N. F. Q. Yuan, Z. Huang, C.-w. Cho, S. H. Lee, Y. S. Hor, K. T. Law, R. Lortz, Nematic topological superconducting phase in Nb-doped $Bi_2Se_3$. *npj Quantum Mater.* **2**, 59 (2017).
27. T. Asaba, B. J. Lawson, C. Tinsman, L. Chen, P. Corbae, G. Li, Y. Qiu, Y. S. Hor, L. Fu, L. Li, Rotational symmetry breaking in a trigonal superconductor Nb-doped $Bi_2Se_3$. *Phys. Rev. X* **7**, 011009 (2017).
28. L. Fu, Odd-parity topological superconductor with nematic order: Application to $Cu_xBi_2Se_3$. *Phys. Rev. B* **90**, 100509 (2014).
29. M. Kriener, K. Segawa, Z. Ren, S. Sasaki, Y. Ando, Bulk superconducting phase with a full energy gap in the doped topological insulator $Cu_xBi_2Se_3$. *Phys. Rev. Lett.* **106**, 127004 (2011).
30. H. Won, K. Maki, D-wave superconductor as a model of high-$T_c$ superconductors. *Phys. Rev. B* **49**, 1397–1402 (1994).
31. G. E. Volovik, Superconductivity with lines of gap nodes: Density of states in the vortex. *JETP Lett.* **58**, 469–473 (1993).
32. A. Vorontsov, I. Vekhter, Nodal structure of quasi-two-dimensional superconductors probed by a magnetic field. *Phys. Rev. Lett.* **96**, 237001 (2006).
33. B. J. Lawson, Y. S. Hor, L. Li, Quantum oscillations in the topological superconductor candidate $Cu_{0.25}Bi_2Se_3$. *Phys. Rev. Lett.* **109**, 226406 (2012).
34. B. J. Lawson, P. Corbae, G. Li, F. Yu, T. Asaba, C. Tinsman, Y. Qiu, J. E. Medvedeva, Y. S. Hor, L. Li, Multiple Fermi surfaces in superconducting Nb-doped $Bi_2Se_3$. *Phys. Rev. B* **94**, 041114 (2016).
35. K. Willa, R. Willa, K. W. Song, G. D. Gu, J. A. Schneeloch, R. Zhong, A. E. Koshelev, W.-K. Kwok, U. Welp, Nanocalorimetric evidence for nematic superconductivity in the doped topological insulator $Sr_{0.1}Bi_2Se_3$. *Phys. Rev. B* **98**, 184509 (2018).
36. Y. Qiu, K. N. Sanders, J. Dai, J. E. Medvedeva, W. Wu, P. Ghaemi, T. Vojta, Y. San Hor, Time reversal symmetry breaking superconductivity in topological materials. arXiv:1512.03519 (2015).
37. C. Q. Han, H. Li, W. J. Chen, F. Zhu, M.-Y. Yao, Z. J. Li, M. Wang, B. F. Gao, D. D. Guan, C. Liu, C. L. Gao, D. Qian, J.-F. Jia, Electronic structure of a superconducting topological insulator Sr-doped $Bi_2Se_3$. *Appl. Phys. Lett.* **107**, 171602 (2015).
38. P. A. Lee, Localized states in a d-wave superconductor. *Phys. Rev. Lett.* **71**, 1887–1890 (1993).
39. M. J. Graf, S.-K. Yip, J. A. Sauls, D. Rainer, Electronic thermal conductivity and the Wiedemann-Franz law for unconventional superconductors. *Phys. Rev. B* **53**, 15147–15161 (1996).
40. L. Taillefer, B. Lussier, R. Gagnon, K. Behnia, H. Aubin, Universal heat conduction in $YBa_2Cu_3O_{6.9}$. *Phys. Rev. Lett.* **79**, 483–486 (1997).
41. K. Nakayama, H. Kimizuka, Y. Tanaka, T. Sato, S. Souma, T. Takahashi, S. Sasaki, K. Segawa, Y. Ando, Observation of two-dimensional bulk electronic states in the superconducting topological insulator heterostructure $Cu_x(PbSe)_5(Bi_2Se_3)_6$: Implications for unconventional superconductivity. *Phys. Rev. B* **92**, 100508 (2015).
42. M. P. Smylie, H. Claus, U. Welp, W. K. Kwok, Y. Qiu, Y. S. Hor, A. Snezhko, Evidence of nodes in the order parameter of the superconducting doped topological insulator $Nb_xBi_2Se_3$ via penetration depth measurements. *Phys. Rev. B* **94**, 180510 (2016).


**Acknowledgments:** A.R. would like to thank F. Herman for the valuable discussions. **Funding:** This work was funded by the Deutsche Forschungsgemeinschaft (DFG; German Research Foundation) under CRC 1238-277146847 (A04 and B01) and under Germany's Excellence Strategy–Cluster of Excellence Matter and Light for Quantum Computing (ML4Q) EXC 2004/1-390534769. A.R. acknowledges the support of Fundação de Amparo à Pesquisa do Estado de São Paulo (FAPESP) project 2018/18287-8, Fundação para o Desenvolvimento da UNESP (FUNDUNESP) process 2338/2014-CCP, and ICTP-SAIFR FAPESP grant 2016/01343-7.

**Author contributions:** Y.A. conceived the experiment and A.R. constructed the theory. L.A. and Z.W. performed sample growth and characterizations. L.A. measured the specific heat and thermal conductivity with help from T.L. and L.A. T.L. and Y.A. analyzed the data. Y.A., A.R., and L.A. wrote the manuscript with inputs from all authors. **Competing interests:** The authors declare that they have no competing interests. **Data availability:** All data needed to evaluate the conclusions in the paper are present in the paper and/or the Supplementary Materials. Additional data related to this paper may be requested from the authors.

Submitted 7 July 2019
Accepted 4 December 2019
Published 28 February 2020
10.1126/sciadv.aay6502

**Citation:** L. Andersen, A. Ramires, Z. Wang, T. Lorenz, Y. Ando, Generalized Anderson's theorem for superconductors derived from topological insulators. *Sci. Adv.* **6**, eaay6502 (2020).

# Generalized Anderson's theorem for superconductors derived from topological insulators

Lionel Andersen, Aline Ramires, Zhiwei Wang, Thomas Lorenz and Yoichi Ando

*Sci Adv* **6** (9), eaay6502.
DOI: 10.1126/sciadv.aay6502